Journal of Crystal Growth 335 (2011) 51–57

Contents lists available at SciVerse ScienceDirect

Journal of Crystal Growth

journal homepage: www.elsevier.com/locate/jcrysgro

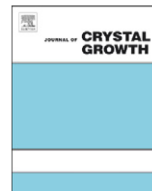

The influence of N_2/H_2 and ammonia N source materials on optical and structural properties of AlN films grown by plasma enhanced atomic layer deposition

Mustafa Alevli, Cagla Ozgit, Inci Donmez, Necmi Biyikli *

UNAM Institute of Materials Science and Nanotechnology, Bilkent University, Ankara 06800, Turkey

ARTICLE INFO

Article history:
Received 17 May 2011
Received in revised form
30 August 2011
Accepted 4 September 2011
Communicated by C. Caneau
Available online 10 September 2011

Keywords:
A1. Crystal structure
A1. Self-limited growth
A3. Atomic layer deposition
B1. Aluminum nitride

ABSTRACT

The influence of N_2/H_2 and ammonia as N source materials on the properties of AlN films grown by plasma enhanced atomic layer deposition using trimethylaluminum as metal source has been studied. The ϖ-2Θ grazing-incidence X-ray diffraction, high resolution transmission electron microscopy, and spectroscopic ellipsometry results on AlN films grown using either NH_3 or N_2/H_2 plasma revealed polycrystalline and wurtzite AlN layers. The AlN growth rate per cycle was decreased from 0.84 to 0.54 Å/cycle when the N source was changed from NH_3 to N_2/H_2. Growth rate of AlN remained constant within 100–200 °C for both N precursors, confirming the self-limiting growth mode in the ALD window. Al–Al bond was detected only near the surface in the AlN film grown with NH_3 plasma. AFM analysis showed that the RMS roughness values for AlN films grown on Si(100) substrates using NH_3 and N_2/H_2 plasma sources were 1.33 nm and 1.18 nm, respectively. The refractive indices of both AlN films are similar except for a slight difference in the optical band edge and position of optical phonon modes. The optical band edges of the grown AlN films are observed at 5.83 and 5.92 eV for ammonia and N_2/H_2 plasma, respectively. According to the FTIR data for both AlN films on sapphire substrates, the E_1(TO) phonon mode position shifted from 671 cm^{-1} to 675 cm^{-1} when the plasma source was changed from NH_3 to N_2/H_2.

© 2011 Elsevier B.V. All rights reserved.

1. Introduction

The low-temperature growth of ultra thin III-nitride films with homogeneous and well-controlled film thickness down to the sub-nanometer scale, high chemical stability, and suitable step coverage is necessary to enable the integration of III-nitride device layers in silicon CMOS microelectronic circuits. Among the III-nitride compounds, aluminum nitride (AlN) is a promising material for CMOS integration due to its unique optical and electrical properties [1,2]. AlN features a promising optically transparent window around 6.2 eV for ultraviolet and visible light emitting diodes, optical coatings, and multi-tandem solar cells [1,3,4]. Moreover, AlN can be a good template for the fabrication of short wavelength emitters and detectors owing to its thermal stability and high thermal conductivity. As a result of these properties, a significant amount of effort has been devoted towards the synthesis of epitaxial, polycrystalline, and amorphous grade AlN thin films [1,4–7]. While high-temperature grown epitaxial AlN films are used in active electronic and opto-electronic device layers, polycrystalline and amorphous AlN films grown at CMOS-compatible temperatures are widely used as dielectrics and passivation layers for microelectronic devices [8,9]. AlN has also the potential of enhancing the III–V device performances when used as the passivation layer by eliminating the surface recombination and Fermi level pinning.

Chemical vapor deposition (CVD) of AlN films is generally carried out using trimethyl-aluminum (TMA) as the metal precursor in combination with NH_3 or N_2/H_2 as N source materials [10,11]. However, ammonia requires high temperatures for efficient cracking (typically above 500 °C) while N_2/H_2 needs even higher growth temperatures [12]. Atomic layer deposition is a unique type of CVD growth technique, which enables low-temperature growth of nitride thin films with sub-monolayer thickness control [13,14]. To overcome the limited N precursor cracking efficiency at such low temperatures, rf plasma process can be utilized [15,16]. Plasma-enhanced ALD (PEALD) offers a potential solution in order to obtain AlN at temperatures significantly lower than thermal ALD processes due to the increased levels of reactive nitrogen [1,5]. In remote-plasma ALD process, only non-metal precursors are activated in order to avoid cracking of metal precursors. In the ideal PEALD growth, both organometallic Al-precursor molecules and reactive nitrogen species are

* Corresponding author. Tel.: +90 312 290 3556; fax: +90 312 266 4530.
E-mail address: biyikli@unam.bilkent.edu.tr (N. Biyikli).

0022-0248/$ - see front matter © 2011 Elsevier B.V. All rights reserved.
doi:10.1016/j.jcrysgro.2011.09.003

chemisorbed on the film surface. During this self-limiting growth mode, gas-phase reactions are eliminated due to the separate injection of precursors while thermal decomposition of the metal precursor is avoided due to low growth temperatures.

There has been a few studies on PEALD of AlN thin films [10,15,17]. While the material properties of PEALD AlN films deposited above 200 °C using N_2 and NH_3 plasma have been investigated, no comparative study has been done so far to study the effect of N_2 and NH_3 plasma on PEALD grown AlN films with deposition temperatures lower than 200 °C [10]. The main motivation of this study is to study the influence of the N_2/H_2 and NH_3 plasma on the growth of AlN films in the self-limited growth region. Structural and optical properties of ALD-grown AlN films were comparatively investigated. From now on, we are going to name AlN films grown by NH_3 plasma AlN(NH_3) and those grown by N_2/H_2 plasma AlN(N_2/H_2).

2. Experimental procedures

Aluminum nitride films were grown in a Cambridge Nanotech Fiji F200 remote rf-plasma ALD reactor with a base pressure of 0.2 Torr. Pre-cleaned Si (100), Si (111), sapphire, and quartz substrates were used throughout the experiments. TMA and NH_3 or N_2/H_2 radicals were used as Al and N sources, while Ar was used as the carrier/purging gas. The TMA bubbler temperature was kept at 27 °C. For PEALD, NH_3 and N_2/H_2 gas reactants are excited remotely in the upper part of the reactor within a separate excitation chamber. The generated nitrogen/hydrogen radicals are flown into the growth chamber. The precursor carrier gas flows were set at 60 sccm and 50 sccm for TMA and N-source gases, respectively. Initially, the substrate temperature was fixed at 185 °C and plasma power set to 300 W, and then the TMA exposure time and plasma times were varied in order to obtain the pulse times for saturation, i.e. 0.05 s for TMA, 40 s for NH_3/Ar and N_2/H_2/Ar plasmas. Then, fixing the TMA exposure at 0.1 s (or 0.05 s) and the NH_3/Ar and N_2/H_2/Ar plasma duration at 40 s, the growth temperature was varied between 100 °C and 400 °C to obtain the ALD window, i.e. from 100 to 200 °C. Finally, 90 nm thick films were grown at 185 °C using 0.1 s (or 0.05 s) for TMA exposure and 40 s for the NH_3/Ar and N_2/H_2/Ar plasma duration to investigate the influence of N source materials on the optical and structural properties.

Characterization measurements of ~90 nm thick AlN(NH_3) and AlN(N_2/H_2) were carried out with the following techniques. Surface and bulk compositions of AlN films were determined by X-ray photoelectron spectroscopy (XPS) utilizing Thermo Scientific instruments with AlK_α radiation in an analysis chamber with 151.2 eV pass energy. Grazing incidence angle X-ray diffraction (GIXRD) measurements were performed using a Philips X'Pert MRD diffractometer with a CuKα radiation in order to analyze the film microstructure and extract phase information at ~0.3° tilt. High-resolution transmission electron microscopy (HR-TEM) imaging was performed in a Tecnai G2 F30 TEM (FEI). Cross sectional TEM specimens were prepared by focused ion beam (FIB Nova 600i Nanolab – FEI), where Pt was used to bond the sample to the carrier. Surface morphology was characterized by atomic force microscopy (AFM) using an Asylum Research, MFP-3D instrument in contact mode with a Si tip. Room temperature transmission measurements were performed with a UV–vis–near infrared spectrometer (Cary Varian 100 UV-vis spectrometer), which includes a built-in phase-sensitive detection and signal processing for the appropriate wavelength regions. Film thickness and refractive index measurements were performed using a J.A.Woollam spectroscopic ellipsometer with a xenon light source. The ellipsometric data of angles (Ψ (65, 70, 75), Δ) in the spectral range of 300–1000 nm were used to calculate the thicknesses of the AlN films and growth rates were calculated by dividing the film's thickness by the number of ALD cycles. Fourier transform infrared (FTIR) spectroscopy was used to investigate the phonon modes in the films. Infrared measurements in reflection geometry were taken using an FTIR spectrometer (Bruker Vertex 70) with a mirror optics microscope (hyperion microscope) and a liquid nitrogen cooled HgCdTe detector. FTIR spectra were taken over the frequency range of 400–7500 cm^{-1} (25–1.33 μm) with a spectral resolution of 4 cm^{-1} at room temperature. All IR reflection spectra were taken under normal incidence light arrangement in order to minimize anisotropy effects. A gold mirror on glass was used as a reference sample for normalization procedure.

3. Results and discussion

3.1. Self-limited atomic layer deposition characteristics

A set of experiments was performed to identify in the temperature range of 100–400 °C the ALD window that produced self-limiting growth. One cycle for depositing AlN films consisted of the following parameters. TMA was pulsed for 0.05 s (N_2/H_2 plasma) and 0.1 s (NH_3 plasma), and assumed to adsorb on the surface active sites to form $Al(CH_3)_x$. Note that the deposition rate increased with increasing TMA dose until 0.05 s, where the growth rate saturated for both N sources. 50 sccm of N_2/H_2 or NH_3 plasma were injected for 40 s with 200 sccm Ar carrier and are expected to react with $Al(CH_3)_x$ to form chemisorbed AlN and released CH_4 groups [14]. 10 s purge times were inserted after the TMA and N_2/H_2–NH_3 steps to eliminate any possible gas-phase reactions. Plasma power was set to 300 W and turned on before the N_2/H_2–NH_3 flow and off before the TMA pulse injection in each cycle. Fig. 1 shows the dependence of the growth rate on the growth temperature of the NH_3 and N_2/H_2 plasma grown AlN films and suggests that growth rate below 200 °C remains almost constant at 0.84 Å/cycle for AlN(NH_3), and at 0.54 Å/cycle for AlN(N_2/H_2). The fact that the growth rate stays constant with increasing growth temperature supports the interpretation of decomposition of TMA occurring on the surface only and a growth mechanism controlled by the self limited surface reactions. Radicals produced in N_2/H_2 and NH_3 plasmas are different and

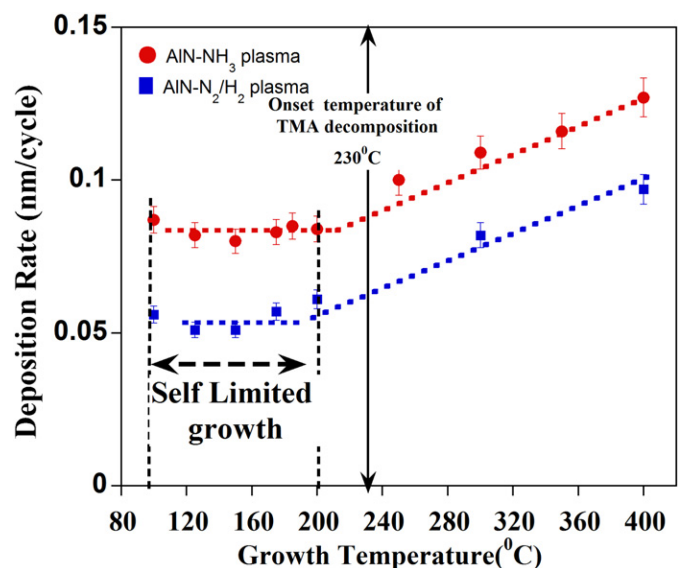

Fig. 1. Dependence of AlN(NH_3) and AlN(N_2/H_2) films growth rate on growth temperature. These films are grown on Si(100).

we assume that they are not equivalent in terms of their reactivities with TMA such as adsorbing Al and desorbing CH_3. The growth rates for $AlN(N_2/H_2)$ samples is lower than those for $AlN(NH_3)$ for all growth temperatures due to the difference in the reactivity of the radicals [18]. In particular, for $AlN(NH_3)$ films, N radicals are expected to be not only N but also NH, NH_2 and NH_3, which might contribute to the AlN growth [19].

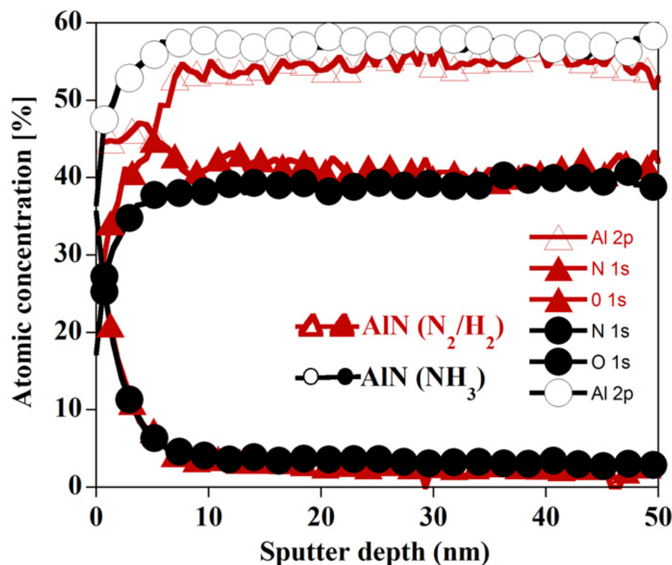

Fig. 2. XPS depth profile of $AlN(NH_3)$ and $AlN(N_2/H_2)$ films. Relative atomic concentrations of aluminum, nitrogen, and oxygen vs. sputtering depth.

3.2. Stoichiometry, structural film analysis, and surface morphology

We have analyzed the elemental composition of AlN films using XPS. Fig. 2 shows an XPS depth profile of Al, N, and O for AlN films. The carbon contamination was completely removed after 5 s sputter cycle and therefore is not shown here. There is 30% atomic concentration of oxygen at the film surface, which drops to a level of 2–3% atomic concentration at 8–10 nm into the film. It was reported in the literature that a 5–10 nm thick Al_2O_3 layer formed when AlN film is exposed to air, based on ellipsometry measurements [20]. We did see a 0.3–0.4 nm thick Al_2O_3 layer according to our X-ray reflection measurement experimental data fitting, which is much thinner than the layer thickness reported in Ref. [20]. The atomic concentration of aluminum decreased and nitrogen increased slightly when N_2/H_2 plasma was used instead of NH_3 plasma. The slightly more metal-rich composition for $AlN(NH_3)$ films was also confirmed by the Al2p sub-peak observed in high resolution scan. Al2p and N1s peaks were fitted using one or two sub-peaks as presented in Fig. 3. The Al2p photoelectron peaks at 73.42 and 73 eV are attributed to Al–N bonds for NH_3 and N_2/H_2 plasma and the peak at 72.3 eV is attributed to Al–Al bonding within the NH_3-plasma film [21]. The N1s spectra in Figs. 3(b) and 3 (d) were deconvoluted into 2 subpeaks with binding energies of ~396 and ~397.8 eV. The strongest peak at 396 eV is characteristic for N1s in the N–Al bond and the small peak at 397.8 eV(397.4 eV for $AlN(N_2/H_2)$ plasma) might be attributed to Al–O–N bond [21]. There is no sign of

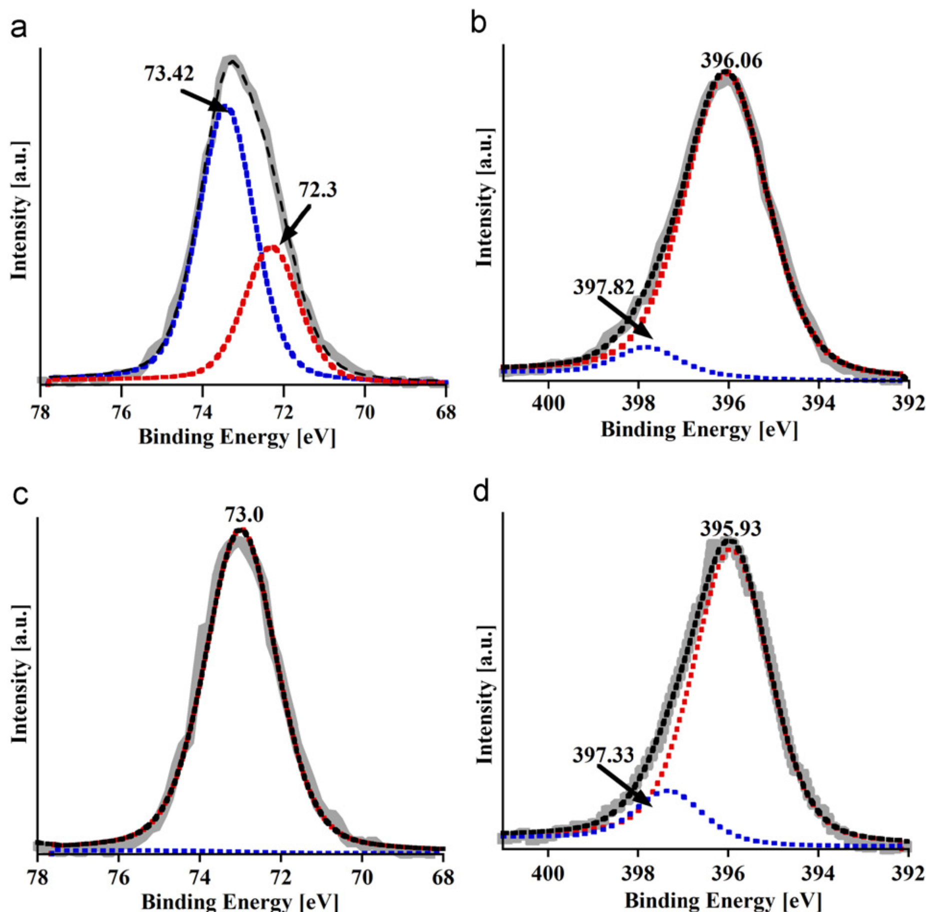

Fig. 3. Core level XPS of Al2p and N1s of (a), (b) $AlN(NH_3)$, and (c),(d) $AlN(N_2/H_2)$ films.

physisorbed nitrogen (N–N bond) or H-related impurities, which could originate from a N_2/H_2 or NH_3 plasma in the XPS analysis of the Al2p and N1s photoelectron peaks. Although our experiments were carried out at a temperature as low as 185 °C, XPS measurements reveal no hydrogen or carbon related impurities such as -NH_x, N–C, and OH^- in both AlN films, which clearly indicate effectively saturated surface reactions of TMA and NH_3 or N_2/H_2 plasma during the deposition process [20,22]. Further experiments such as Rutherford backscattering spectroscopy and elastic recoil detection time of flight need to be done to observe the atomic concentration of H radicals extracted from nitrogen plasma sources [17].

In order to explore the influence of the two different N sources on the crystal structure of AlN films, GIXRD patterns of two AlN films deposited in the self-limited growth region were compared. The GIXRD scans shown in Fig. 4 for the as-deposited films using both plasma source materials indicate that these films crystallize into a polycrystalline form with wurtzite phase. The GIXRD patterns of both films indicate that their diffraction patterns are well matched with the hexagonal AlN structure, and similar X-ray diffraction peaks were observed for both films. Moreover, it has been concluded that our films possess a homogenous hexagonal structure without any phase mixing, i.e. cubic phase, from the GIXRD data.

Fig. 5 (a–d) show the AFM surface morphologies of AlN films deposited on Si(100) with NH_3 plasma (a and b) and N_2/H_2 plasma (c and d). The root mean square (RMS) roughnesses of these films were 1.33 nm (AlN(NH_3)) and 1.18 nm (AlN(N_2/H_2)). The mean grain size (deduced from the Gwyddion image analysis program) for these samples are 6.5 nm and 6.3 nm, respectively [23]. Even though mean grain size values were similar, surface morphologies of AlN films presented here were different. The AFM analysis revealed that the use of N_2/H_2 plasma slightly improves surface roughness and decreases the grain size. Through studying the AFM roughness and grain size on different substrates, our investigation showed that the use of N_2/H_2 plasma is incrementally decreasing the RMS roughness and decreasing the grain size. The average RMS values and grain size were similar, at around 1.1 nm and 6 to 7 nm for different substrates including Si, sapphire, and quartz. Another important outcome of the AFM data is that the uniform material coverage on the substrate surface is shown to be very good in the self-limited growth region.

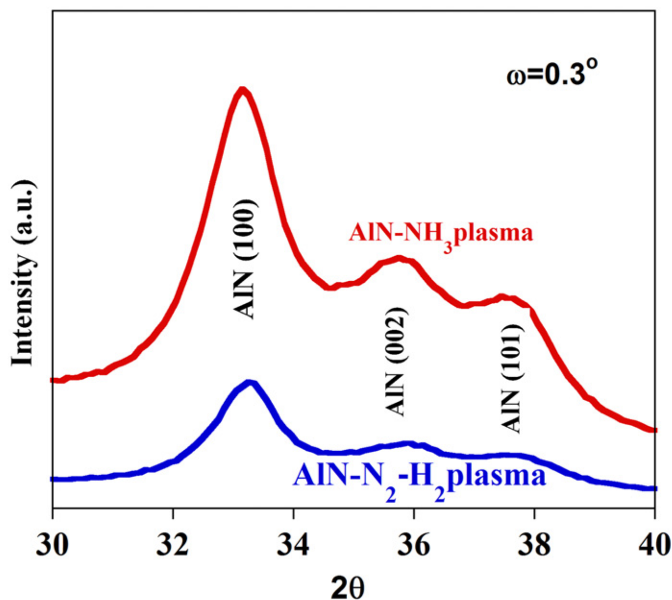

Fig. 4. GIXRD patterns for ~90 nm thick AlN(NH_3) and AlN(N_2/H_2) films grown on Si(100) at 185 °C.

The formation of crystalline structure and interfacial layer was studied by cross-sectional TEM imaging of AlN films. Fig. 5(e–h) show cross sectional HR-TEM images of both films. Both AlN films are composed of nanocrystallites of dimensions less than ~10 nm, and no amorphous phase was observed. There is an ultra-thin interfacial layer less than ~0.5 nm thick between the as-deposited film and the Si substrate, which might be attributed to an SiO_x layer formed at the Si/AlN interface for both AlN films (Fig. 5g and h). This would agree with the increased oxygen concentration at the substrate surface in XPS measurements. HR-TEM images for both AlN films clearly exhibited lattice fringes directing in different planes, which confirms the polycrystalline structure obtained from GIXRD data.

3.3. Optical properties

Normal incidence optical transmittance and absorption measurements were performed to investigate the optical transparency and absorption properties of the self-limited grown AlN films. Transmission measurements of the films were carried out between 190 and 800 nm, allowing an investigation of the band-edge transition in the UV range, and of the impurity-related transition bands in the visible range, as shown in Fig. 6. According to the onset of transmission spectra, AlN(N_2/H_2) has a higher transmission onset commencing at 188 nm, whereas the onset of the transparency red-shifted to 193 nm for AlN(NH_3) sample. At 300 nm, transmission increases to a maximum value and remains nearly constant in both samples until 800 nm. Absorption bands centered at ~250 nm, below the optical band gap, were associated with the vacancy-related defects V_N and V_{Al} [24] (see Fig. 6a inset). The metallic Al–Al bonding deduced from XPS high resolution spectra for AlN(NH_3) also implies the existence of nitrogen vacancies with the more pronounced absorption band at 250 nm for this sample. It was observed that there is a widening of the absorption edge up to 300 nm, where this band was associated to the oxygen related defect, which was detected in the XPS data as well [25]. However, the oxygen concentration was about the same for both samples as confirmed by XPS data, and no direct correlation between oxygen impurities and the ~280 nm absorption band was found. Fig. 6b shows a plot of the squared absorption coefficient, α^2, as a function of wavelength in order to determine the energy of the optical band edge for our AlN films. The optical band edge can be determined by extrapolating the tangential line to the wavelength axis in the $\alpha^2 d^{-2}$ vs. λ plot. The optical band edge was observed at 5.83 eV and 5.92 eV for AlN(NH_3) and AlN(N_2/H_2) samples, respectively.

Fig. 7 depicts the variation of refractive index as a function of wavelength for AlN films. It was observed that AlN(NH_3) displayed a refractive index of 1.939, while AlN(N_2/H_2) film showed a refractive index of 1.930, both data measured at 533 nm. When compared to single-crystal quality refractive index value (n=2.1 at 533 nm), our films have almost 93% of the bulk value, which is approximately equal to the relative density compared to the bulk material. No significant change is observed in the refraction index of both AlN films due to the different "N" source materials. This means that the refractive indexes of AlN films remain unchanged. The values of refractive index obtained from spectroscopic ellipsometry were found to be in the range of 1.9–2.1, which is in good agreement with the GIXRD and HR-TEM data, which indicate that our AlN films are polycrystalline. The extinction coefficients were 3.3×10^{-3} for the AlN(NH_3) film and 5.6×10^{-3} for AlN(N_2/H_2) over the chosen wavelength range, and constant for $\lambda > 300$ nm for both AlN films. The low extinction coefficients indicate that

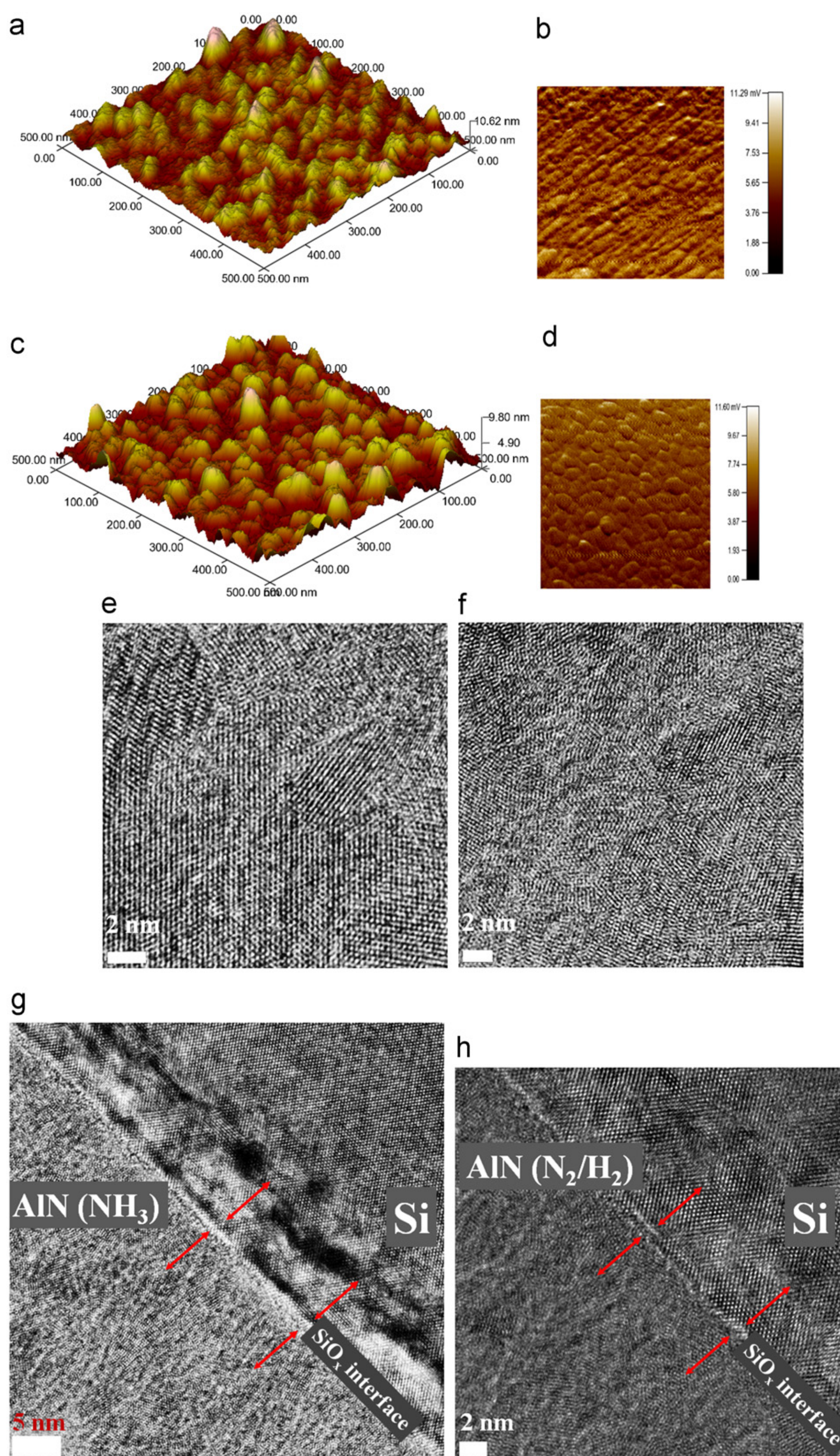

Fig. 5. AFM surface images of ~90 nm thick AlN(NH_3) and AlN(N_2/H_2) films on Si(100) in (a and c) height trace (b and d) lateral trace modes. Cross sectional high resolution TEM images for (e) AlN(NH_3) and (f) AlN(N_2/H_2) films on Si(100). (g and h) Ultra-thin interfacial layer, which might be attributed to SiO_x layer formed at the Si/AlN interface for both AlN films.

the films are transparent in this wavelength region and in good agreement with the optical transmission data.

FTIR spectra obtained from AlN samples are shown in Fig. 8. The spectral range displayed corresponds to the transverse and longitudinal-optical-phonon energy range. For the AlN films grown on Si(100) and Si(111), the reflectance shows a pronounced broad Reststrahlen band bracketed by the transverse and longitudinal optical phonon energies. The reflectance spectra

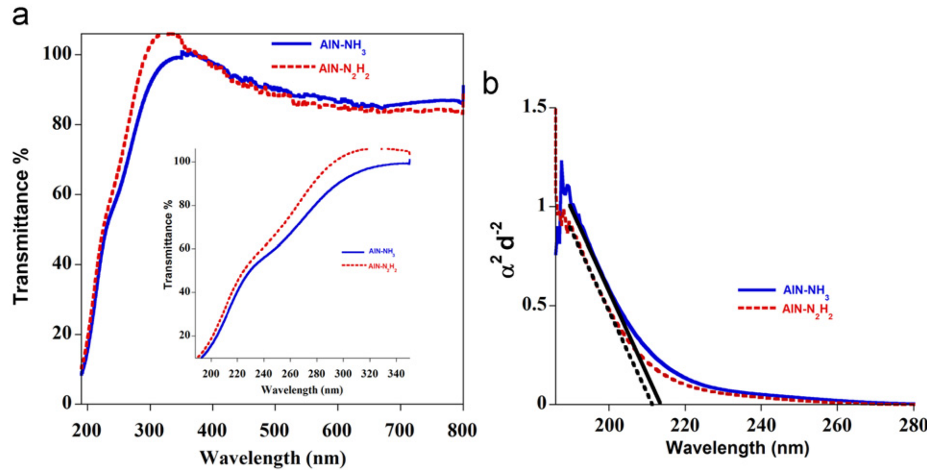

Fig. 6. (a) Transmission spectra of AlN(NH_3) and AlN(N_2/H_2) films on quartz. The inset shows the absorption band positioned at 250 nm. (b) The square of the product of the absorption coefficient as a function of wavelength for AlN films.

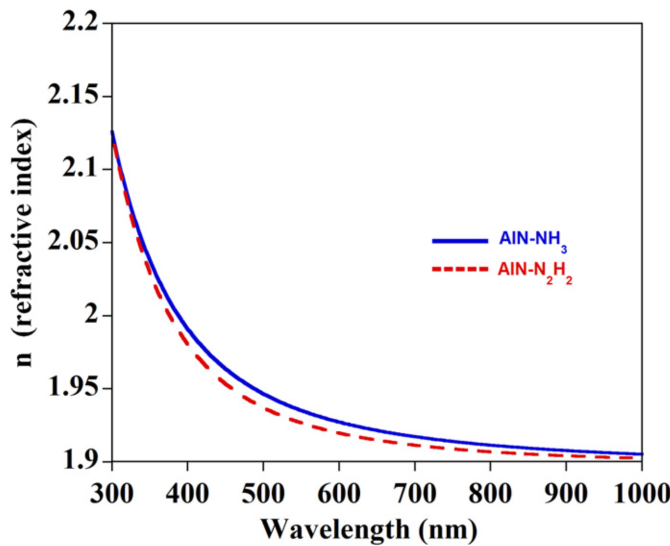

Fig. 7. Variation of refractive index n of AlN(NH_3) and AlN(N_2/H_2) films as a function of incident photon wavelength.

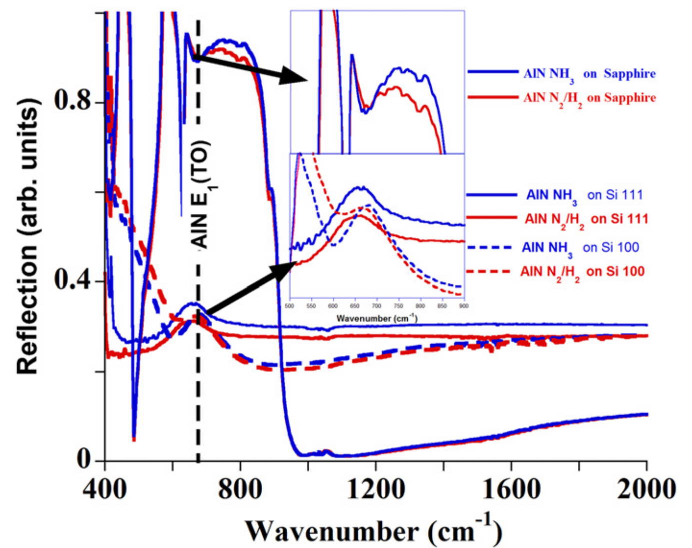

Fig. 8. Reflection of AlN(NH_3) and AlN(N_2/H_2) films. The inset shows a magnified detail of restrahlen bands in AlN films and the evidence of E_1(LO) observed in AlN film grown on sapphire.

of films grown on Si substrates evolve to show the same maximum, which are most closely associated with E_1(TO) and A_1(LO) phonons. The peak position is centered around 680 cm^{-1} for Si (100) and 662 cm^{-1} for Si (111), which might be due to the difference in lattice mismatch between the substrate and the film [26]. It is hard to determine the exact E_1(TO) phonon position without modeling the IR spectra. However, the reflection data of both AlN films on sapphire substrate clearly show the infrared active E_1(TO) phonon position. The phonon position was found to be 671 cm^{-1} for the AlN(NH_3) film and 675 cm^{-1} for the AlN(N_2/H_2) film. According to the literature[27], the E_1(TO) phonon peak position in the stress-free film is 673 cm^{-1}, and residual stress in the deposited films can lead to a higher wavenumber shifting in FTIR peaks. Based on this statement, the use of NH_3 plasma as N source material might have caused less stress in the deposited film. No additional information was obtained in the high wavenumber range above 1200 cm^{-1}. FTIR spectra for both AlN films on various substrates show no evidence of A_1(LO) phonon of AlN at 890 cm^{-1}. Based on our XPS and FTIR measurement results, there is no evidence of hydrogen adsorbed to AlN in the IR data (Al–H stretch ~1800 cm^{-1}) [28]. This again confirms the efficient removal of the methyl groups.

4. Conclusions

In this study, the influence of NH_3 and N_2/H_2 as N source materials on the structural and optical properties of PEALD-grown AlN films has been investigated. Growth of AlN films demonstrated that PEALD is a viable tool for the growth of group III-Nitride alloys at temperatures as low as 100 °C. XPS and FTIR results reveal no hydrogen and carbon impurities in both AlN films, which indicate complete self-limited reactions of TMA and NH_3, N_2/H_2 plasma. AFM data demonstrated that the film coverage on the substrate surface is shown to be continuous and homogeneous in the self limited growth region. No significant change was observed in the refractive index of both AlN films due to the different N source materials but the position of phonon modes and optical band edge was located at different positions.

Another significant output of this study is that the use of NH_3 precursor is leading to an Al rich structure at the very film surface.

Acknowledgments

This work was performed at UNAM supported by the State Planning Organization (DPT) of Turkey through the National Nanotechnology Research Center Project. Authors would like to acknowledge K. Mizrak and M. Guler from UNAM for TEM sample preparation and HR-TEM measurements. N.B. acknowledges support from Marie Curie International Re-integration Grant (Grant # PIRG05-GA-2009–249196). M.A. acknowledges the financial support from TUBITAK (Project no: 232.01–660/4835).

References

[1] K. Reid, A. Dip, S. Sasaki, D. Triyoso, S. Samavedam, D. Gilmer, C.F.H. Gondran, Thin Solid Films 517 (2009) 2717–2718.
[2] H. Conrad, J.U. Schmidt, W. Pufe, F. Zimmer, T. Sandner, H. Schenk, H. Lakner, Proceedings of SPIE (2009) 7362J.
[3] K. Ueno, A. Kobayashi, J. Ohta, H. Fujioka, H. Amanai, S. Nagao, H. Horie, Physica Status Solidi RRL 2–3 (2008) 58–60.
[4] J. Wu, Applied Physical Letters 106 (2009) 011101.
[5] D. Riihela, M. Ritala, R. Matero, M. Leskela, J. Jokinen, P. Haussalo, Chemical Vapor Deposition 2 (1996) 277.
[6] F. Hajakbari, M.M. Larijani, M. Ghoranneviss, M. Aslaninejad, A. Hojabri, Japanese Journal of Applied Physics 49 (2010) 095802.
[7] C. Mirpuri, S. Xu, J.D. Long, K. Ostrikov, Journal of Applied Physics 101 (2007) 024312.
[8] M. Bosund, P. Mattila, A. Aierken, T. Hakkarainen, H. Koskenvaara, M. Sopanen, V.M. Airaksinen, H. Lipsanen, Applied Surface Science 256 (2010) 7434–7437.
[9] D. Kueck, P. Leber, A. Schmidt, G. Sperenza, E. Kohn, Diamond and Related Materials 19 (2010) 932–935.
[10] J. Dendooven, D. Deduytsche, J. Mussschoot, R.L. Vanmeirhaeghe, C. Detavernier, Journal of the Electrochemical Society 157 (2010) G111–G116.
[11] K. Kim, N. Kwak, S. Lee, Electronic Materials Letters 5 (2009) 83–86.
[12] X. Liu, S. Ramanathan, E. Lee, T.E. Seidel, Materials Research Society Symposium Proceedings (2004), p. D1.9.1.
[13] M. Rittala, M. Leskela, Atomic Layer Deposition, in: H.S. Nalwa (Ed.), Hand Book of Thin Film Materials, Academic Press, New York, 2002, pp. 103–153.
[14] H. Kim, J. Vac, Sci. Tech. A 21 (2003) 2231.
[15] Y.J. Lee, Journal of Crystal Growth 266 (2004) 568–572.
[16] Z. Bochkour, P. Tristant, E. Thune, C. Dublanche-Tixier, C. Jaoul, R. Guinebretiere, Surface and Coating Technology 205 (2011) S586–S591.
[17] M. Bosund, T. Sajavaara, M. Laitinen, T. Huhtio, M. Putkonen, V.M. Airaksinen, H. Lipsanen, Applied Surface Science 257 (2011) 7827–7830.
[18] D.C. Jordan, I.S.T. Tsong, D. Smith, B.J. Wilkens, R.B. Doak, Applied Physical Letters 77 (2000) 3030.
[19] O. Danielsson, E. Janzen, Journal of Crystal Growth 253 (2003) 26–37.
[20] R. Dalmau, R. Collazo, S. Mita, Z. Sitar, Journal of Electronic Materials 36 (2006) 414–419.
[21] L. Rosenberger, R. Baird, E. McCullen, E. Auner, G. Shreve, Surface and Interface Analysis 40 (2008) 1254–1261.
[22] Y. Lee, S. Kang, Thin Solid Films 446 (2004) 227.
[23] Gwyddion is a free software and a part of General Public License(GNU). More information on 〈http://gwyddion.net/〉.
[24] M. Badylevich, S. Shamulia, V. Afanasev, A. Stesmans, Y. Fedorenko, C. Zhao, Journal of Applied Physics 104 (2008) 093713–093714.
[25] M. Strassburg, J. Senawiratne, N. Dietz, U. Haboeck, A. Hoffmoann, V. Noveski, R. Dalmau, R. Schlesser, Z. Sitar, Journal of Applied Physics 96 (2004) 5870.
[26] J.X. Zhang, H. Cheng, Y.Z. Chen, A. Uddin, S. Yuan, S.J. Geng, S. Zhang, Surface and Coatings Technology 198 (2005) 68–73.
[27] C. Wetzel, E. Haller, H. Amano, I. Akasaki, Applied Physical Letters 68 (1996) 2547–2549.
[28] D.C. Bertolet, H. Liu, J.W. Rogers, Chemistry of Materials 5 (1993) 1814–1818.